The action potential-evoked sarcoplasmic reticulum calcium release is impaired in *mdx* mouse muscle fibres

Christopher E. Woods, David Novo, Marino DiFranco and Julio L. Vergara

Department of Physiology, UCLA School of Medicine, Los Angeles, CA 90095, USA

The *mdx* mouse, a model of the human disease Duchenne muscular dystrophy, has skeletal muscle fibres which display incompletely understood impaired contractile function. We explored the possibility that action potential-evoked Ca^{2+} release is altered in *mdx* fibres. Action potential-evoked Ca^{2+}-dependent fluorescence transients were recorded, using both low and high affinity Ca^{2+} indicators, from enzymatically isolated fibres obtained from extensor digitorum longus (EDL) and flexor digitorum brevis (FDB) muscles of normal and *mdx* mice. Fibres were immobilized using either intracellular EGTA or *N*-benzyl-*p*-toluene sulphonamide, an inhibitor of the myosin II ATPase. We found that the amplitude of the action potential-evoked Ca^{2+} transients was significantly decreased in *mdx* mice with no measured difference in that of the surface action potential. In addition, Ca^{2+} transients recorded from *mdx* fibres in the absence of EGTA also displayed a marked prolongation of the slow decay phase. Model simulations of the action potential-evoked transients in the presence of high EGTA concentrations suggest that the reduction in the evoked sarcoplasmic reticulum Ca^{2+} release flux is responsible for the decrease in the peak of the Ca^{2+} transient in *mdx* fibres. Since the myoplasmic Ca^{2+} concentration is a critical regulator of muscle contraction, these results may help to explain the weakness observed in skeletal muscle fibres from *mdx* mice and, possibly, Duchenne muscular dystrophy patients.

(Resubmitted 15 January 2004; accepted after revision 2 March 2004; first published online 5 March 2004)
Corresponding author J. L. Vergara: Department of Physiology, UCLA School of Medicine, Los Angeles, CA 90095, USA. Email: jvergara@mednet.ucla.edu

The absence of dystrophin causes Duchenne muscular dystrophy (DMD), the most common debilitating genetic disorder affecting boys (for a review, see Emery, 2002). It has been shown that DMD is caused by mutations in the dystrophin gene, located on the X-chromosome, which results in the improper expression of the protein dystrophin (Hoffman *et al.* 1987*a*).

Much of our knowledge of the properties of dystrophin, and the pathological consequences of its absence, comes from experimental evidence obtained studying the *mdx* mouse, an animal model of DMD that also lacks the expression of dystrophin protein. Importantly, although the pathophysiology of the *mdx* mouse is not identical to that of the DMD patient (Gillis, 1999), it has been reported that muscle fibres from both DMD patients and *mdx* mice exhibit significantly reduced active force development (Wood *et al.* 1978; Coirault *et al.* 1999). Using the *mdx* mouse model, it has been shown that the absence of dystrophin leads to the absence of the dystrophin-associated glycoprotein complex (DAG) (for review see Emery, 2002). In an attempt to explain the overall weakness of *mdx* muscle, it has been proposed that the DAG complex serves as a membrane anchor and that without it, the overall membrane integrity is compromised and the Ca^{2+} homeostasis of the dystrophic muscle is disrupted, leading to necrosis of the muscle (Turner *et al.* 1988). Although these results are controversial (for a review see Gillis, 1999), neither this mechanism nor any other proposed to date seems to account for the impaired force production of single fibres (Watchko *et al.* 2002; for a review see Emery, 1993).

Under physiological conditions, impairment in sarcoplasmic reticulum (SR) Ca^{2+} release in response to an action potential (AP) could cause skeletal muscle fibre weakness since Ca^{2+} is the trigger for contraction and the dependence of tension development on myoplasmic free Ca^{2+} concentration is very steep (Godt, 1974; Fink *et al.* 1990). Previous authors have investigated this possibility by recording AP-evoked Ca^{2+} transients. However, these authors reported only minimal differences in the kinetic properties and no significant differences in the amplitude of transients recorded from normal and *mdx*

 DOI: 10.1113/jphysiol.2004.061291

muscles (Turner *et al.* 1988; Head, 1993; Tutdibi *et al.* 1999).

In this paper, we have revisited the issue of evoked Ca^{2+} signalling in normal and *mdx* muscle fibres. We used low and high affinity Ca^{2+} indicators, in the presence of intracellular concentrations of either EGTA or *N*-benzyl-*p*-toluene sulphonamide (BTS) (Cheung *et al.* 2002; Shaw *et al.* 2003) to block contraction, in order to record AP-evoked Ca^{2+} transients without movement artifacts. Moreover, by measuring AP-evoked Ca^{2+} transients using a low affinity indicator in the presence of an EGTA concentration ([EGTA]) of 5 mM, we were able to infer the properties of SR Ca^{2+} release (Song *et al.* 1998; Novo *et al.* 2003) in normal and *mdx* fibres. Our results demonstrate that the peak free $[Ca^{2+}]$ changes recorded in response to AP stimulation are significantly smaller in *mdx* muscle fibres compared to normal counterparts. We propose that an alteration in the SR Ca^{2+} release flux in dystrophic muscle fibres may be responsible for this decrease. A preliminary version of this work has been presented to the Biophysical Society (Woods *et al.* 2003).

Methods

Isolation of fibres

All experiments were carried out according to the guidelines laid down by the UCLA Animal Care Committee. Single muscle fibres were enzymatically isolated from flexor digitorum brevis (FDB) and extensor digitorum longus (EDL) muscles dissected from normal (C57BL/10SnJ) and *mdx* (C57BL/10ScSn-mdx/J) (Jackson Laboratories, ME, USA) mice. Both of these muscles have been reported to be composed mostly of fast-twitch (type II) fibres (Parry & Parslow, 1981; Raymackers *et al.* 2000). All experiments were done in 8- to 18-week-old normal and post-necrotic *mdx* mice (McArdle *et al.* 1995). Mice were deeply anaesthetized with halothane (loss of righting reflex) and killed by cervical dislocation. Muscles were removed, stored in cold (5°C) Tyrode solution (see below) and utilized within 30 min.

The digestion and dissociation protocol is a modification of those described in the literature (Head *et al.* 1990; Szentesi *et al.* 1997). Each muscle was placed in a Sylgard-bottomed Petri dish with its tendons held in place by pins and bathed in 0 Mg^{2+}, 0 Ca^{2+} Tyrode solution supplemented with 262 units ml^{-1} of collagenase Type IV (Sigma, St Louis, MO, USA) and 0.5 mg ml^{-1} of bovine serum albumin. The muscles were incubated for 45 min at 37°C under mild agitation. Collagenase activity was stopped by washing the muscle with 0 Mg^{2+}, Ca^{2+} Tyrode solution at 37°C. The muscle mass was gently sucked in and out of a fire-polished Pasteur pipette until muscle fibres were isolated. For FDB fibres, the average diameter and length were ~30 μm and ~300 μm, respectively. For EDL fibres, the average diameter and length were ~60 μm and ~6 mm, respectively. We have found that immediately following this dissociation procedure, only very few of the large number of fibres isolated actively twitched in response to external electrical stimulation when bathed in external solutions containing 2.0 mM $[Ca^{2+}]$. However, after incubation for 30 min in L-15 media (Sigma) supplemented with 0.1 mg ml^{-1} penicillin–streptomycin (Sigma) in an O_2 saturated environment at 25°C, approximately 25% of the fibres responded to external stimulation with vigorous twitches. Only this population of fibres was used. All of these observations and procedures applied identically to both normal and dystrophic muscle fibres.

Solutions

The internal solution contained (mM): 140 potassium aspartate; 20 K-Mops; 2.5 or 5 $MgSO_4$, 5 Na_2-PCr, 5 K-ATP, 5 dextrose, 2.5 glutathione, and 0.1 mg ml^{-1} creatine phospho-kinase. The [EGTA] of the internal was adjusted to 5 or 10 mM as specified in text. In the presence of 5 mM EGTA, the free $[Mg^{2+}]$ of the internal solution was calculated, using the Maxchelator program (Bers *et al.* 1994), to be 77 μM and 0.53 mM, for 2.5 and 5 mM total Mg^{2+}, respectively. For experiments in the absence of EGTA, only 5 mM total Mg^{2+} was used, and the free $[Mg^{2+}]$ under these conditions was 0.6 mM. The composition of the external Tyrode solution was (mM): 145 NaCl, 5 KCl, 2 $CaCl_2$, 1 $MgCl_2$, 10 Na-Mops, 10 dextrose. The 0 Mg^{2+}, 0 Ca^{2+} Tyrode solution was as above without added Ca^{2+} and Mg^{2+}. In some experiments, *N*-benzyl-*p*-toluene sulphonamide (BTS), an inhibitor of the myosin II ATPase, was added to the external solution at a concentration of 50 μM as we found that this was the minimum concentration necessary to completely arrest shortening of the fibre in response to AP stimulation. All solutions were adjusted to an osmolarity of 300 mosmol kg^{-1} of water and a pH of 7.4. Experiments were performed at 22°C.

Electrophysiological techniques

The electrophysiological method used for enzymatically dissociated EDL fibres was similar to the triple Vaseline gap technique previously described for mechanically dissected

frog muscle fibres (Hille & Campbell, 1976; Palade & Vergara, 1982; Kim & Vergara, 1998). The main change was the use of a silicone compound (Chemplex 825, NFO Technologies, KS, USA) to construct the seals, instead of petroleum jelly compounds, and the inclusion of 1% fetal calf serum (FCS, Irvine Scientific) in the external solution to further improve the tolerance of the fibres to Chemplex 825 (Szentesi *et al.* 1997). The fibres were straightened across the gaps, maintained at slack sarcomere length (∼2 μm) and loaded with internal solution (see below) through the cut ends. The holding potential of the central pool was set at −95 mV.

FDB muscle fibres were transferred to an optical chamber (DiGregorio *et al.* 1999) containing Tyrode solution and impaled with two micropipettes. These micropipettes were placed ∼150 μm apart in un-stretched fibres with a sarcomere length of ∼2 μm, as shown in the phase contrast image in Fig. 1*A*. The first one was a high resistance micropipette (pipette 1, Fig. 1*A*), which had ∼40 MΩ resistance when filled with 3 M KCl, and the second one was a low resistance micropipette (pipette 2, Fig. 1*A*), which had a resistance of ∼30 MΩ when filled with internal solution. Pipette 1 was used to record the transmembrane potential (V_m). No current was passed through this electrode. Pipette 2 was used to load the fibre with internal solution, to maintain its resting potential, and to stimulate it. Both micropipettes were connected to a TEV-200A amplifier (Dagan, Minneapolis, MN, USA). To rule out differences in the passive electrical properties between normal and *mdx* fibres used in our experiments, we compared the current necessary to set the V_m to −90 mV and found that, from a large population of twitching fibres, including those reported in Results, in the absence of BTS, 11.7 ± 1 and 12.3 ± 1 nA of current was necessary in normal and *mdx* fibres, respectively ($n = 49$ fibres from 12 normal mice; $n = 43$ fibres from 14 *mdx* mice) and in the presence of BTS, 33 ± 7 and 35 ± 5 nA of current was necessary for normal and *mdx* fibres, respectively ($n = 12$ fibres from 5 normal mice; $n = 28$ fibres from 6 *mdx* mice). In comparison to the steady-state holding current, APs were elicited using supra-threshold current pulses of 0.5 ms duration and 0.2−0.5 μA amplitude (upper and lower limits for experiments in both the presence and absence of BTS), with no observed difference in the magnitude of the pulses necessary for AP stimulation between normal and *mdx* fibres. For FDB fibre experiments described in this report, the resting V_m was adjusted to the values indicated in the figure legends with the aid of constant hyperpolarizing current injection. The area enclosed by the white square in Fig. 1*A* is shown

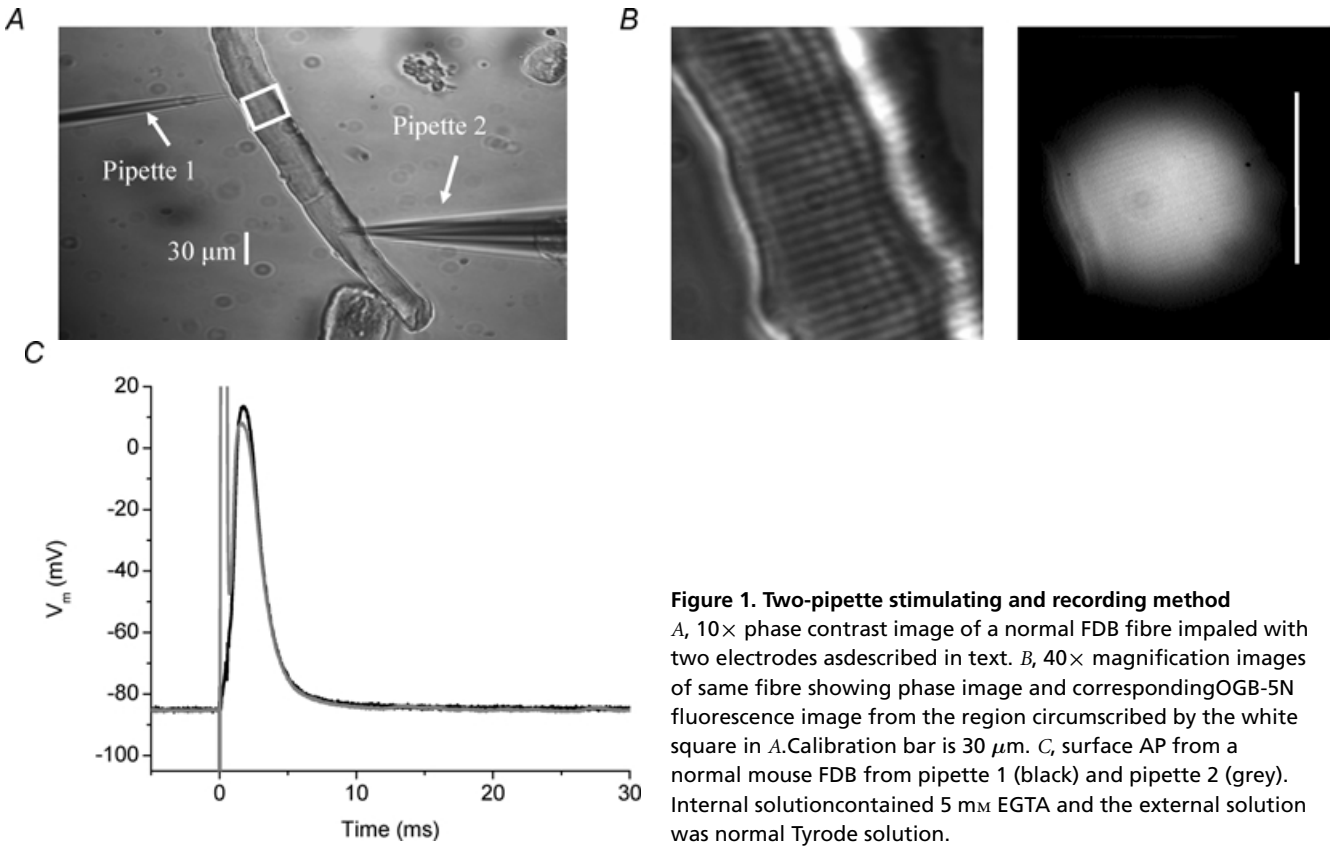

Figure 1. Two-pipette stimulating and recording method
A, 10× phase contrast image of a normal FDB fibre impaled with two electrodes asdescribed in text. *B*, 40× magnification images of same fibre showing phase image and correspondingOGB-5N fluorescence image from the region circumscribed by the white square in *A*.Calibration bar is 30 μm. *C*, surface AP from a normal mouse FDB from pipette 1 (black) and pipette 2 (grey). Internal solutioncontained 5 mM EGTA and the external solution was normal Tyrode solution.

at higher magnification in Fig. 1*B* in order to illustrate the striation pattern of the fibre (left panel) and the disc-shaped illumination area where the fluorescence signals were recorded from in a typical fibre. Figure 1*C* shows the APs recorded at both pipettes superimposed. As expected, the recordings from pipette 2 show a saturating stimulus artifact that prevents the recording of the initial part of the rising phase of the AP. As the artifact could not be eliminated, we included a second microelectrode (pipette 1) to faithfully acquire the AP. As can be seen Fig. 1*C*, the record of the AP from pipette 1 does not show the artifact. All AP records from FDB fibres in the paper were recorded by pipette 1.

The FDB fibres were loaded passively with the internal solution by a mechanism comparable to that described for patch clamp experiments (Pusch & Neher, 1988; Mathias *et al.* 1990; Wang *et al.* 1999). Accordingly, the loading rates of relevant pipette constituents were calculated using the measured value for the pipette resistance, published values for the diffusion coefficients and resistivity, and an estimated cell volume for a FDB muscle fibre of typical dimensions and geometry, assuming that 70% of the fibre volume is free for diffusion of exogenous constituents without binding (Melzer *et al.* 1987). The resistivity for the internal solution was assumed to be 240 Ω cm (Pusch & Neher, 1988), and the values for the diffusion coefficients were 1.8×10^{-5}, 9×10^{-6}, and 5.6×10^{-6} cm^2 s^{-1}, for K^+ ions, fluorescein (a molecule of comparable molecular weight to EGTA) and Oregon Green 488 BAPTA-5N (OGB-5N), respectively (Pusch & Neher, 1988; Woods & Vergara, 2002). Assuming that the diffusion coefficient of EGTA equals that of fluorescein, our calculations show that 30 min after impalement, the intracellular concentrations of K^+, EGTA and OGB-5N were 94, 78 and 60%, respectively, of their pipette values. At 60 min after impalement the corresponding percentages were: 99.8, 95 and 84%, respectively. A final caveat to these results is that, for at least the Ca^{2+} indicator, binding to intracellular constituents most likely occurs as reported previously (Maylie *et al.* 1987; DiFranco *et al.* 2002). In fact, the resting fluorescence continued to rise throughout the experiment (∼1 h) without reaching a steady-state value, as would be expected for a process of diffusion with binding (Maylie *et al.* 1987).

In agreement with the theoretical calculations for loading, by 30 min following impalement, the properties of $\Delta F/F$ transients (see below) were stable within 8% of each other (standard deviation/mean). In addition, in the presence of at least 5 mM EGTA, fibre movement was arrested by 30 min as judged both by the absence of movement artifacts in the electrical and optical records, as well as by visual inspection of the fibre imaged with 100× magnification on the screen of a monitor. Thus, all optical measurements were initiated 30 min after fibre impalement. After recordings were started, the fluorescence transients were stable, typically for 30 more minutes and in some cases for as long as 90 more minutes. In addition, $\Delta F/F$ transients measured near pipette 2 and at the ends of the fibre had similar properties. Thus, after the equilibration period, the concentrations of solutes in the fibre were assumed to approximate that of the internal solution in pipette 2, with the caveat that binding to internal constituents of the fibre may prevent the attainment of a true steady state.

Ca^{2+} measurements and data analysis

$[Ca^{2+}]$ was measured using the cell-impermeant forms of the Ca^{2+} indicators OGB-5N (Molecular Probes, Eugene, OR, USA) or Oregon Green 488 BAPTA-1 (OGB-1, Molecular Probes). The concentration of OGB-5N in the internal solution was 500 μM and that of OGB-1 was 50 μM. The equilibrium dissociation constants (K_d values) and the F_{max}/F_{min} ratio (R) of OGB-5N and OGB-1 were determined *in vitro* using protocols similar to those described elsewhere (Escobar *et al.* 1997; Nagerl *et al.* 2000). Briefly, the free $[Ca^{2+}]$ of a set of standard solutions (pCa 9 to 3, in increments of 0.5 pCa units) was measured and adjusted with custom-made Ca^{2+}-sensitive electrodes. These were made of a small plastic (PVC) tube (10–20 mm long, 0.7 mm in diameter) of which 0.5–1 mm of one side was filled with a 1 : 1 mixture of 10% (w/w) Ca^{2+}-selective ionophore II (Fluka/Sigma-Aldrich, St Louis, MO, USA) plus 2% (w/w) sodium tetraphenylborate dissolved in 2-nitrophenyloctyl ether and 8–10% (w/w) polyvinylchloride dissolved in tetrahydrofuran (THF). A thin Ca^{2+}-selective membrane formed after evaporation of the THF, and the electrodes were stored at room temperature for at least 2 days before use. Electrodes were used only if they exhibited linear (Nernstian) behaviour in the pCa range of 3–8 with a slope of at least 27 mV pCa^{-1} and a measurable responsivity to pCa 9. Both Ca^{2+} dyes were dissolved in every standard solution to a concentration of 20 μM and the fluorescence of a sample of each solution (10 μl) was measured using the optical set-up described below. The fluorescence values were used to generate fluorescence *versus* pCa calibration curves which were fitted with eqn (2) from Escobar and collaborators (Escobar *et al.* 1997). For the particular batch of OGB-5N (lot No. 34B2-1) used in this report, K_d and R were 48 ± 7 μM and 11 ± 0.26, respectively. For OGB-1 these values were 155 ± 29 nM and 11 ± 1.1,

respectively. The free $[Ca^{2+}]$ of the internal solutions were determined by interpolation from the OGB-1 calibration curve. Fluorescence measurements of the internal solution samples containing 20 μM OGB- (with or without EGTA) were made and pCa values were interpolated from the dye calibration curves. In so doing, the free $[Ca^{2+}]$ of the internal solution was estimated to be 64 ± 5 nM in the absence of EGTA and 2 ± 1 nM in the presence of 5–10 mM EGTA. Using the flash photolysis method (Escobar *et al.* 1997; Nagerl *et al.* 2000), we calculated the *in vitro* association and dissociation rate constants for OGB-5N to be: $k_{on} = 1.57\ \mu M^{-1}\ s^{-1}$ and $k_{off} = 7520\ s^{-1}$, respectively. For EGTA, we adopted previously reported values of $K_d = 71$ nM, $k_{on} = 10.5\ \mu M^{-1}\ s^{-1}$ and $k_{off} = 0.75\ s^{-1}$ (Nagerl *et al.* 2000).

Spatially averaged AP-evoked fluorescence transients were recorded with OGB-5N or OGB-1 using either an inverted microscope (FDB experiments) or an upright microscope (EDL experiments). Both optical set-ups have been described previously (Kim & Vergara, 1998; DiGregorio *et al.* 1999). The fluorescence transients were normalized to $\Delta F/F$ units and characterized according to the following parameters as previously described (Vergara & DiFranco, 1992; DiFranco *et al.* 2002): $(\Delta F/F)_{peak}$; duration, expressed as the full-duration–half-maximum (FDHM); and delay to peak (t_p), measured from the initiation of the rising phase of the transient to $(\Delta F/F)_{peak}$. The decay phase of the OGB-5N transients was fitted, using a least-squares fitting routine (Origin 6.1, Microcal, Northhampton, MA, USA), to the following biexponential function:

$$y = A_{fast} \exp(-t/\tau_{fast}) + A_{slow} \exp(-t/\tau_{slow}) \quad (1)$$

where t is the time (in ms) after the peak of the transient, and A_{fast} and A_{slow} are fitted amplitudes of the fast and slow components, the sum of which cannot exceed the $(\Delta F/F)_{peak}$.

Assuming that OGB-5N was at equilibrium with the free peak $[Ca^{2+}]$ and that the resting fluorescence of the indicator in the fibres was equal to F_{min}, the free peak $[Ca^{2+}]$ underlying the $(\Delta F/F)_{peak}$ values of the OGB-5N transients could be estimated according to the following equation:

$$\text{Peak}[Ca^{2+}] = K_d((\Delta F/F)_{peak})/((R-1) - (\Delta F/F)_{peak}) \quad (2)$$

The validity of these assumptions for fluorescence transients recorded with low affinity indicators, such as OGB-5N, has been demonstrated previously (Escobar *et al.* 1995, 1997). The values for R for OGB-5N were measured *in vivo* as described elsewhere (Vergara & DiFranco, 1992; Vergara *et al.* 2001) and found to be 11 ± 3 ($n = 3$), comparable to the *in vitro* condition (see above).

To determine the AP-evoked SR Ca^{2+} release flux, OGB-5N $\Delta F/F$ transients recorded in the presence of high internal [EGTA] were analysed using the closed form equilibrium approximation of Song and collaborators (eqn (5) in Song *et al.* 1998) and a single compartment kinetic model including EGTA, the Ca^{2+} indicator, and Ca^{2+} as the reactants with rate constants determined *in vitro*. The model generated $\Delta F/F$ transients according to the following equation:

$$\Delta F(t)/F = ([BCa(t)] - [BCa(0)])/([B_{tot}]/(R-1) + [BCa(0)]) \quad (3)$$

where $[BCa(t)]$ is the time-dependent concentration of the Ca-bound indicator and $[B_{tot}]$ is the total concentration of indicator in the cell. The initial concentration of the Ca-bound indicator ($[BCa(0)]$) was calculated according the following formula:

$$[BCa(0)] = ([B_{tot}][Ca^{2+}(0)])/(K_d + [Ca^{2+}(0)]) \quad (4)$$

where $[Ca^{2+}(0)]$ is the resting (initial) $[Ca^{2+}]$ taken as the value in the internal solution in the presence of 5 mM [EGTA]. The kinetics of the Ca^{2+} release flux ($J(t)$) was described by the equation:

$$J(t) = J_{max}(1 - \exp(-t/\tau_{on})^N (A_1 \exp(-t/\tau_{off1}) + A_2 \exp(-t/\tau_{off2}) + A_3 \exp(-t/\tau_{off3})) \quad (5)$$

where t is time (in ms) beginning at the rising phase of the transient. J_{max} (in μM ms^{-1}), A_1, A_2 and A_3 (dimensionless), and τ_{on}, τ_{off1}, τ_{off2} and τ_{off3} (in ms) were adjusted until the time course of the simulated $\Delta F/F$ transient closely approximated the measured transient.

Statistics

For statistical analysis of the data, the parameters described above were determined from a minimum of 10 individual AP-evoked transients per fibre, separated in time such that the $(\Delta F/F)_{peak}$ remained within the stability definition above, and averaged to determine a set of mean values for the fibre. The data are presented as mean ± standard error of the mean (S.E.M.). An unpaired two-population Student's t test, assuming unequal variance, was used to compare the mean fibre values between *mdx* and normal mice. P values are given in the text.

Results

OGB-5N fluorescence transients recorded in FDB muscle fibres with 5 mm EGTA in the internal solution

Our goal was to examine the AP-evoked SR Ca^{2+} release of normal and dystrophic fibres. We chose to record Ca^{2+} transients in fibres loaded with EGTA since this Ca^{2+} buffer at pipette concentrations of $\geq$5 mM is able to effectively arrest fibre movement in response to AP stimulation. As has been suggested previously, the reason for this is that high intracellular [EGTA] constrains the evoked changes in free myoplasmic [Ca^{2+}] to regions near the Ca^{2+} release sites (Pape *et al.* 1995; DiGregorio *et al.* 1999; Novo *et al.* 2003). Empirically, our results reflect this situation because

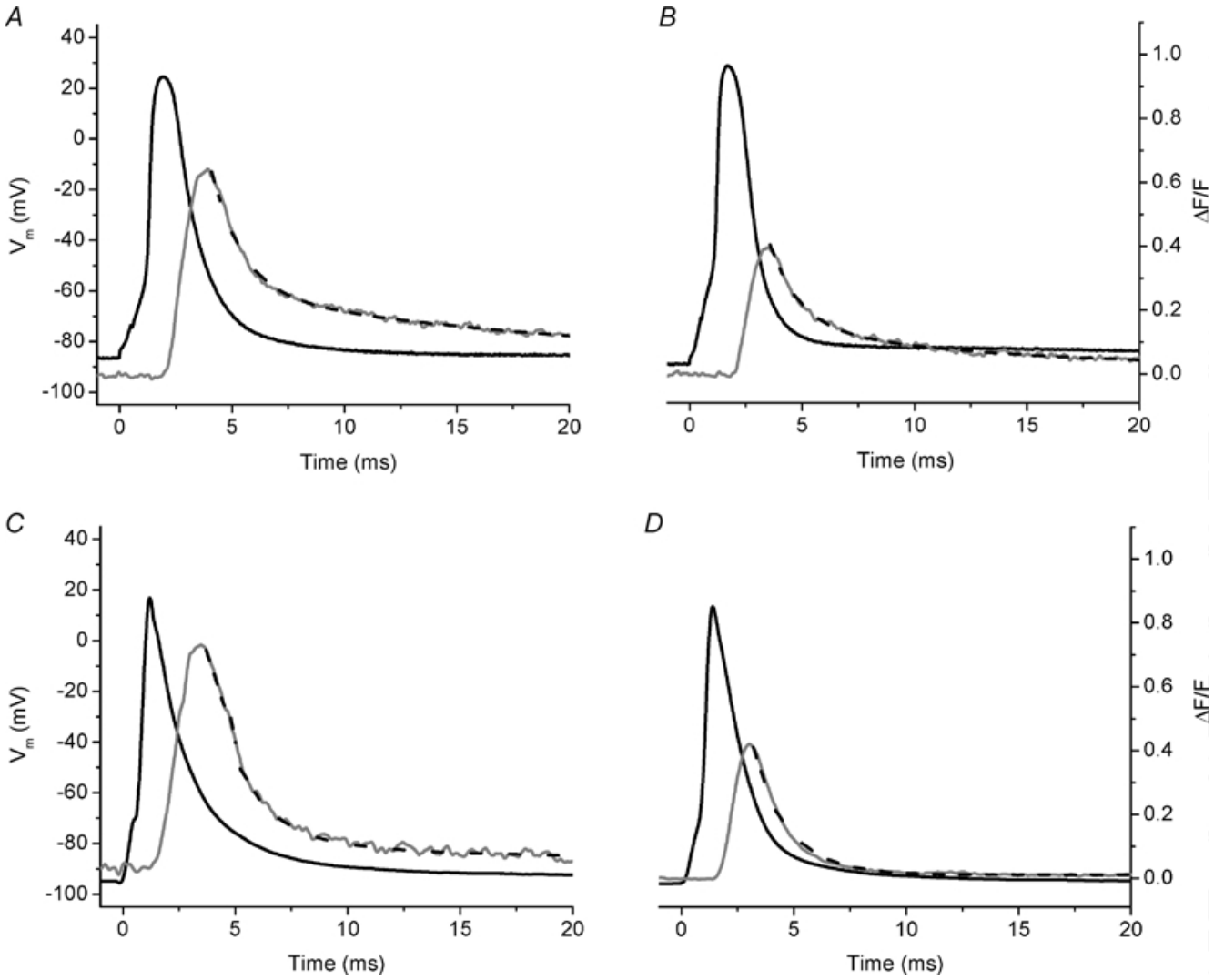

Figure 2. AP-evoked OGB-5N global fluorescent transients from normal and *mdx* single fibres recorded in the presence of 5 mm EGTA in the internal solution

A, AP (black) and evoked OGB-5N fluorescence transient (grey) from an 8-week-old normal mouse FDB fibre. $\Delta F/F_{peak} = 0.66$, $t_p = 1.4$ ms, FDHM = 3.2 ms, $\tau_{fast} = 1.4$ ms, $\tau_{slow} = 23$ ms, $A_1 = 0.44$ ms, $A_2 = 0.25$. Fibre diameter = 30 μm. Resting $V_m = -86$ mV. *B*, AP (black) and evoked OGB-5N fluorescence transient (grey) from an 8-week-old *mdx* mouse FDB fibre. $\Delta F/F_{peak} = 0.39$, $t_p = 1.4$ ms, FDHM = 2.8 ms, $\tau_{fast} = 1.4$ ms, $\tau_{slow} = 10.4$ ms, $A_1 = 0.27$, $A_2 = 0.12$. Fibre diameter = 29 μm. Resting $V_m = -90$ mV. *C*, superimposed AP (black) and evoked OGB-5N fluorescence transient (grey) from a 16-week-old normal mouse EDL fibre. Fibre diameter = 54 μm. Holding potential of the central pool was set to −95 mV. *D*, AP (black) and OGB-5N fluorescence transient (grey) from an 18-week-old *mdx* EDL. Fibre diameter, 65 μm. Holding potential of the central pool was set to −95 mV. The black dashed lines in all panels are the corresponding two-exponential (Figure 2*A* and *B*) and single exponential (Figs 2*C*, *D*) fits to the fluorescence data. For all panels, $t = 0$ corresponds to the onset of stimulation.

Table 1. AP amplitude, OGB-5N transient parameters, and peak [Ca^{2+}] for normal and *mdx* muscle fibres in the presence of 5 mM EGTA in the internal solution

	AP amplitude (mV)	$(\Delta F/F)_{peak}$	Peak [Ca^{2+}] (μM)	t_p (ms)	FDHM (ms)	τ_1 (ms)	τ_2 (ms)	A_{slow}/A_{fast}
Normal FDB	111 ± 4.4	0.72 ± 0.05**	3.7 ± 0.3**	1.8 ± 0.1	3.6 ± 0.2	1.7 ± 0.2*	21 ± 3	0.4 ± 0.05
mdx FDB	108 ± 3	0.41 ± 0.03**	2.1 ± 0.2**	2.0 ± 0.1	4.0 ± 0.2	2.3 ± 0.2*	16 ± 1	0.3 ± 0.03
Normal EDL	92 ± 29	0.80 ± 0.04*	4.1 ± 0.4*	1.5 ± 0.3	2.4 ± 0.4	2.1 ± 0.3	—	—
mdx EDL	100 ± 24	0.40 ± 0.02*	1.9 ± 0.4*	1.7 ± 0.2	3.0 ± 0.8	2.0 ± 0.2	—	—

For FDB fibres: fluorescence transient parameters and peak [Ca^{2+}] were obtained from $n = 9$ fibres from 4 normal mice, and $n = 14$ fibres from 4 *mdx* mice ($n = 6$ fibres from 2 normal mice for and $n = 4$ fibres from 2 *mdx* mice in the absence of BTS, with 2.5 mM total [Mg^{2+}] and the rest obtained in the presence of 50 μM BTS with 5 mM total [Mg^{2+}]). AP amplitudes were obtained from $n = 8$ fibres from 4 normal mice and $n = 14$ fibres from 4 *mdx* mice. For EDL fibres: for both normal and *mdx* mice, all the parameters were obtained from $n = 3$ fibres from 3 mice each. ** Statistical significance between normal and *mdx* fibres within muscle type ($P < 0.0001$); * statistical significance between *mdx* and normal EDL fibres ($P < 0.05$).

fibre movement was blocked. An additional advantage of using sufficiently high [EGTA] is that global fluorescence transients recorded using the low affinity Ca^{2+} indicator OGB-5N can closely track the time course of the SR Ca^{2+} release flux (Song *et al.* 1998; DiFranco *et al.* 2002; Novo *et al.* 2003). Figure 2*A* shows superimposed traces of the surface AP and the evoked OGB-5N transient recorded from a normal FDB fibre with 5 mM EGTA in the internal solution. The OGB-5N transient had a rising phase that reached a $(\Delta F/F)_{peak}$ of 0.66 in a t_p of 1.4 ms and a FDHM of 3.2 ms. Moreover, the decay of the transient displayed an initial rapid phase, followed by a slower decay phase towards baseline. We fitted this decay portion of the $\Delta F/F$ transient with a biexponential function (see Methods) yielding a τ_{fast} of 1.4 ms and a τ_{slow} of 23 ms. The magnitude of the contribution of the fast component was larger than that of the slow component ($A_{slow}/A_{fast} = 0.6$). Figure 2*B* shows corresponding signals recorded from a FDB fibre isolated from an *mdx* mouse. While the AP amplitude is similar to that of a normal mouse (Fig. 2*A*), the $(\Delta F/F)_{peak}$ of the OGB-5N fluorescence transient was 0.39, which is 41% reduced compared to that of the normal transient (Fig. 2*A*). The kinetic features of the $\Delta F/F$ transient were quite similar between the two, with the normal fibres displaying a slightly longer τ_{slow} (1.4 ± 0.2 times), and similar t_p and FDHM (see figure legend for values). Rows 1 and 2 of Table 1 summarize these results from multiple experiments. There was a highly significant $43 \pm 2\%$ decrease in the $(\Delta F/F)_{peak}$ of the AP-evoked OGB-5N transient in *mdx versus* normal FDB fibres. While the τ_{fast} of *mdx* FDB fibres was significantly prolonged, neither the AP amplitude nor any of the other kinetic properties of the OGB-5N transients were significantly different between normal and *mdx* FDB fibres under these conditions. Moreover, we have performed these experiments with the total [Mg^{2+}] set at 2.5 or 5 mM in the internal solution and have observed no difference in the results. Therefore, data from fibres in both conditions have been merged in the Table 1. All FDB experiments presented throughout the rest of the Results section were performed with 5 mM Mg^{2+} in internal solution.

OGB-5N fluorescence transients recorded in EDL fibres with 5 mM EGTA in the cut ends

Since it was possible that the degree of impairment of AP-evoked Ca^{2+} release in *mdx* fibres was dependent on the muscle from which the fibres were derived, we measured evoked OGB-5N transients in the presence of 5 mM EGTA in EDL muscle fibres. The length of these fibres is too long to allow an approximate equilibration of the pipette contents within the fibre in a reasonable time using the microelectrode methodology. Consequently, we used the triple Vaseline gap technique for EDL fibres, instead. Figure 2*C* and *D* shows superimposed records of the AP and the evoked OGB-5N fluorescence transient recorded for either a normal or an *mdx* EDL fibre, respectively, which show that the $(\Delta F/F)_{peak}$ is decreased for the *mdx* transient compared to the normal transient, while the kinetic features of the transients are not different (see figure legend for values). In parallel to the findings for the FDB fibres, the results from multiple experiments demonstrate that the $(\Delta F/F)_{peak}$ of the OGB-5N transient is significantly decreased by $51 \pm 3\%$ in *mdx* compared to normal EDL fibres. Comparison of the $(\Delta F/F)_{peak}$ between normal FDB and EDL fibres (first and third row, Table 1) as well as between *mdx* FDB and EDL fibres (second and fourth row, Table 1), demonstrated no significant difference ($P > 0.5$) within each population. Consequently, by pooling the

results from FDB and EDL fibres shown in Table 1, we calculate an average $45 \pm 6\%$ decrease in the $(\Delta F/F)_{peak}$ of the OGB-5N transients in *mdx* compared with normal muscle fibres ($P < 0.0001$, $n = 14$ fibres from 8 normal mice, $n = 18$ fibres from 8 *mdx* mice). Analogous to the results in FDB fibres, we observed no differences in the kinetic parameters of $\Delta F/F$ transients between normal and *mdx* EDL fibres. However, in contrast to the FDB fibre transients, the decay phase of EDL fibres was best fitted by a single exponential function (Table 1, rows 3 and 4). It can also be observed that the OGB-5N transients from EDL fibres from both normal and *mdx* fibres have briefer FDHM values than the corresponding transients obtained from FDB fibres. These differences may result from differences between EDL and FDB fibres or between the techniques used to load of the fibre with EGTA: the gap isolation technique *versus* the two pipette method. Given the similarity in the $(\Delta F/F)_{peaks}$ between EDL and FDB fibres within strains of fibres, it seems likely, however, that this reflects an intrinsic difference between the two muscles.

OGB-5N fluorescence transients recorded in FDB fibres in the presence of BTS, and in the absence of EGTA

It is possible that the high [EGTA] in the internal solution used in the experiments above, by lowering the intracellular $[Ca^{2+}]$ and artificially increasing the Ca^{2+} buffering, exacerbates an underlying Ca^{2+} signalling abnormality of *mdx* fibres. To test this possibility, we recorded AP-evoked Ca^{2+} transients in the absence of EGTA from normal and *mdx* fibres. In order to block contraction without using EGTA, we bathed the fibre in 50 μM BTS, a potent and specific blocker of force production (Cheung *et al.* 2002; Shaw *et al.* 2003), 50 μM being the minimum concentration of this drug necessary to completely arrest movement of unstretched FDB fibres. While Cheung *et al.* (2002) and Shaw *et al.* (2003) reported no alteration in the Ca^{2+} signalling of frog muscle fibres exposed to BTS, it was important to verify that the properties of both the electrical and Ca^{2+} signals in mammalian fibres were unaltered by BTS. Thus, we first measured AP-evoked Ca^{2+} signals from normal and *mdx* FDB fibres using the conditions for Fig. 2 but in the presence of 50 μM BTS in the external solution (Fig. 3*A* and *B*). It can be observed that 50 μM BTS prolongs the decay phase of the AP in FDB fibres, which is lower than the concentration suggested by Cheung and collaborators which produces a similar effect in frog muscle fibres (Cheung *et al.* 2002). However, this prolongation does not seem to significantly affect the properties of evoked Ca^{2+} signalling in mammalian muscle fibres. The results from these and other experiments demonstrate that $(\Delta F/F)_{peak}$ and the kinetic parameters of OGB-5N fluorescence transients recorded from normal and *mdx* fibres in the presence of 5 mM EGTA and 50 μM BTS do not differ from those of

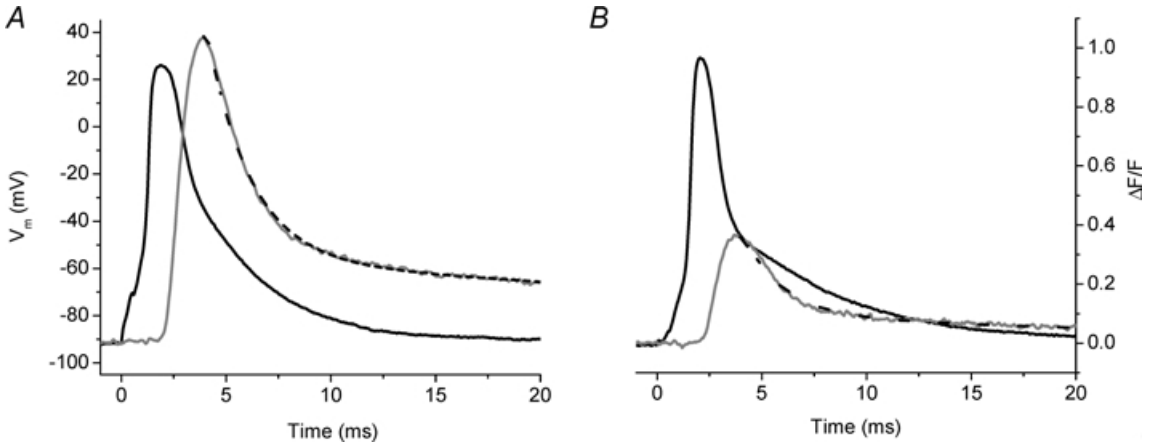

Figure 3. AP-evoked OGB-5N global fluorescent transients from normal and *mdx* single FDB fibres recorded in the presence of 5 mM EGTA in the internal solution and 50 μM extracellular BTS
A, AP (black) and evoked OGB-5N fluorescence transient (grey) from a 14-week-old normal mouse FDB fibre. $\Delta F/F_{peak} = 0.95$, $t_p = 2.1$ ms, FDHM = 3.7 ms, $\tau_{fast} = 1.9$ ms, $\tau_{slow} = 17$ ms, $A_1 = 0.73$, $A_2 = 0.25$. Fibre diameter = 30 μm. Resting $V_m = -96$ mV. *B*, AP (black) and evoked OGB-5N fluorescence transient (grey) from a 13-week-old *mdx* mouse FDB fibre. $\Delta F/F_{peak} = 0.43$, $t_p = 2.0$ ms, FDHM = 3.9 ms, $\tau_{fast} = 1.9$ ms, $\tau_{slow} = 14$ ms, $A_1 = 0.3$, $A_2 = 0.09$. Fibre diameter = 31 μm. Resting $V_m = -92$ mV. The black dashed lines in all panels are the corresponding two-exponential fits to the fluorescence data. For all panels, $t = 0$ corresponds to the onset of stimulation.

transients recorded in the absence of BTS (compare legends of Fig. 3*A* and *B* and Fig. 2*A* and *B*). Therefore, the results obtained from FDB fibres in the presence of 5 mM EGTA in the internal solution, both with and without BTS, were pooled together in Table 1.

The importance of the preceding observations is that they show BTS does not alter AP-induced Ca^{2+} release, thus allowing us to examine whether AP-evoked Ca^{2+} transients recorded from *mdx* fibres were altered with respect to those of normal fibres in the absence of EGTA. Figure 4*A* shows superimposed traces of the membrane AP and the evoked OGB-5N transient recorded from a normal FDB fibre in the absence of EGTA in the internal solution and in the presence of 50 μM BTS in the extracellular solution. As expected, in the absence of EGTA the OGB-5N transient displayed a larger $(\Delta F/F)_{peak}$ (1.1) and a longer FDHM (8.5 ms) than in its presence, while t_p was quite similar (for comparison see Fig. 2*A*). In addition, both τ_{fast} and τ_{slow} (1.9 and 29 ms, respectively) were longer than in the presence of EGTA. This trend is also seen in the

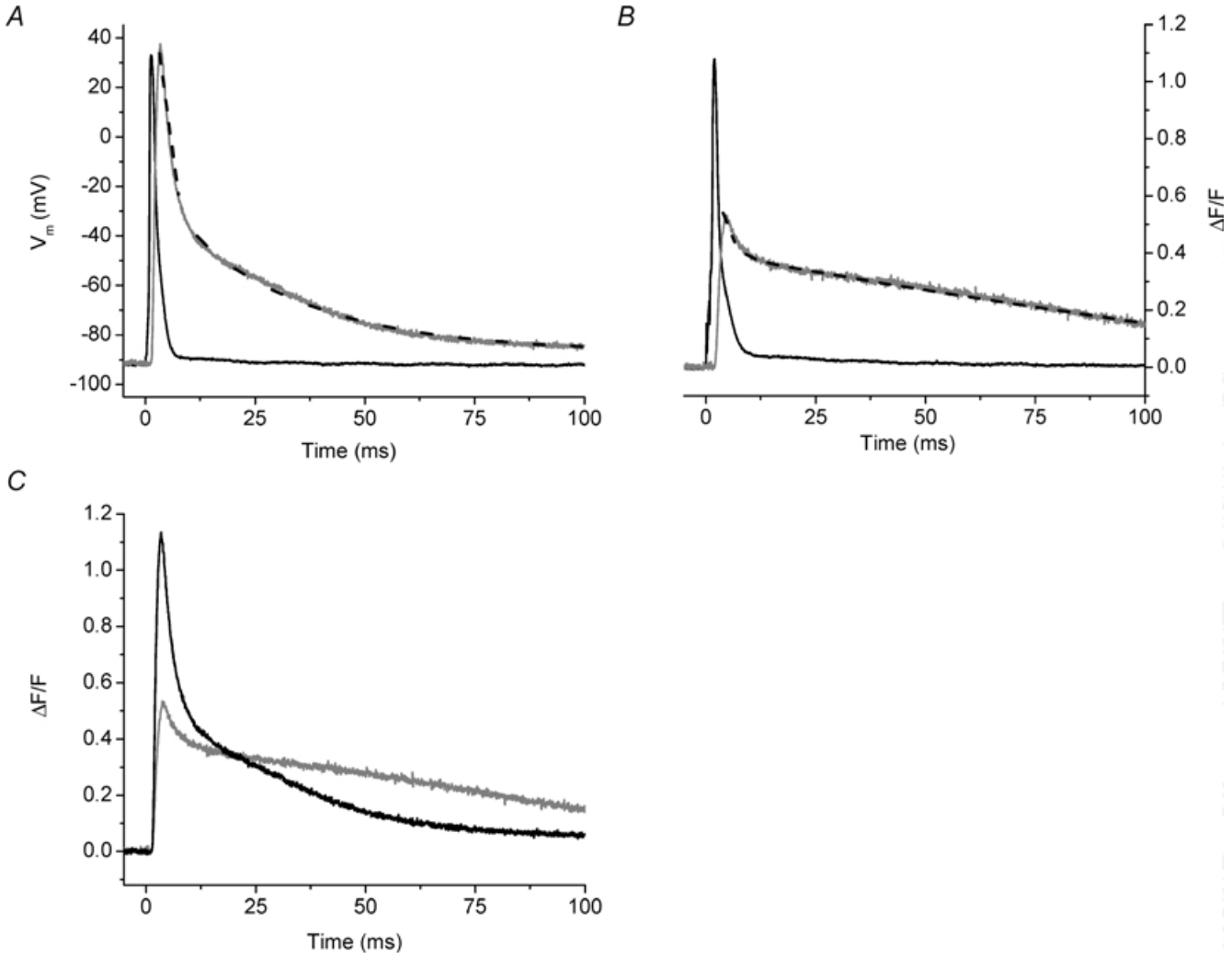

Figure 4. AP-evoked OGB-5N global fluorescent transients from normal and *mdx* single FDB fibres recorded in the absence of EGTA and in the presence of 50 μM extracellular BTS

A, AP (black) and evoked OGB-5N fluorescence transient (grey) from a 13-week-old normal mouse FDB fibre. $\Delta F/F_{peak} = 1.13$, $t_p = 2.0$ ms, FDHM = 8.52 ms, $\tau_{fast} = 1.9$ ms, $\tau_{slow} = 29$ ms, $A_1 = 0.54$, $A_2 = 0.53$ Fibre diameter = 28 μm. Resting $V_m = -92$ mV. *B*, AP (black) and evoked OGB-5N fluorescence transient (grey) from an 8-week-old *mdx* mouse FDB fibre. $\Delta F/F_{peak} = 0.53$, $t_p = 2.4$ ms, FDHM = 53 ms, $\tau_{fast} = 2.1$ ms, $\tau_{slow} = 109$ ms, $A_1 = 0.14$, $A_2 = 0.41$. Fibre diameter = 29 μm. Resting $V_m = -94$ mV. *C*, the normal (black) and the *mdx* (grey) $\Delta F/F$ transients shown in Fig. 4*A* and *B* are shown superimposed. The black dashed lines in panels *A* and *B* are the corresponding two-exponential fits to the fluorescence data. For all panels, $t = 0$ corresponds to the onset of stimulation.

Table 2. OGB-5N transient parameters and peak [Ca^{2+}] for normal and *mdx* muscle fibres in the absence of EGTA

	$(\Delta F/F)_{peak}$	Peak [Ca^{2+}] (μM)	t_p (ms)	FDHM (ms)	τ_1 (ms)	τ_2 (ms)	A_{slow}/A_{fast}
Normal FDB	$1.1 \pm 0.02^{**}$	$6.0 \pm 0.1^{**}$	2.1 ± 0.1	$8.0 \pm 0.5^{**}$	2.3 ± 0.1	$37 \pm 3^{*}$	$1.3 \pm 0.1^{*}$
mdx FDB	$0.64 \pm 0.04^{**}$	$3.3 \pm 0.2^{**}$	2.5 ± 0.1	$48 \pm 6^{**}$	3.0 ± 0.4	$113 \pm 18^{*}$	$2.5 \pm 0.3^{*}$

For experiments, fluorescence transient parameters and peak [Ca^{2+}] were obtained from $n = 5$ FDB fibres from 2 normal mice and $n = 11$ fibres from 2 *mdx* mice. All transients were obtained with 5 mM total [Mg^{2+}]. * Statistical significance between normal and *mdx* FDB fibres ($P < 0.05$); ** statistical significance between normal and *mdx* FDB fibres ($P < 0.0001$)

transient recorded under similar conditions from an *mdx* FDB fibre (Fig. 4*B*). The $(\Delta F/F)_{peak}$ was 0.53, which is a 55% decrease compared to that of the normal transient (Fig. 4*A*), and parallels values observed in the presence of high [EGTA] (Fig. 2*A* and *B*). Surprisingly, while the t_p and τ_{fast} (see figure legend for values) of this transient were similar to those of the normal fibre shown in Fig. 4*A*, the FDHM (53 ms) and τ_{slow} (109 ms) of the *mdx* transient were significantly longer than the corresponding values of the normal transient (Fig. 4*A*). These data suggest that *mdx* fibre transients differ from normal not only in $(\Delta F/F)_{peak}$, but also in the decay phase. The two transients are shown superimposed in Fig. 4*C* to illustrate that at late times (>25 ms), the $\Delta F/F$ transient from the *mdx* fibre was higher than that of the normal fibre, even though its $(\Delta F/F)_{peak}$ was smaller.

Table 2 presents a summary of the properties of the OGB-5N transients obtained without EGTA from *mdx* and normal FDB fibres. Overall, it can be observed that there is a highly significant $42 \pm 4\%$ decrease in the $(\Delta F/F)_{peak}$ of *mdx* fibres under these conditions, which is not statistically different from that observed for OGB-5N transients in the presence of 5 mM EGTA ($P > 0.5$). In contrast to the finding for OBG-5N transients with 5 mM EGTA in the internal solution (Table 1), the FDHMs of *mdx* fibre transients recorded in the absence of EGTA were significantly longer than their normal counterparts ($P < 0.0001$, Table 2). Since both the t_p values and the τ_{fast} values of the *mdx* transients recorded in the absence of EGTA were similar to those of the normal fibre transients (Table 2), while the τ_{slow} and the ratio A_{slow}/A_{fast} were significantly larger (by 3.0 ± 0.8 and 1.9 ± 0.1 times, respectively; $P < 0.05$), this lengthening of the FDHM can most easily be explained by a prolongation of the slow component of the decay phase.

Calculation of the peak [Ca^{2+}] in response to AP stimulation

Making the assumption that OGB-5N is able to track accurately the changes in free [Ca^{2+}] during an AP-evoked SR Ca^{2+} release, we calculated (see Methods) the peak myoplasmic free [Ca^{2+}] which yields the measured $(\Delta F/F)_{peak}$ of the transients and these values are shown in Table 1 (column 3) and Table 2 (column 2). From these data, we calculated that the myoplasmic free peak [Ca^{2+}] was decreased by 46 ± 9 and $45 \pm 4\%$ in the presence of 5 and 0 mM EGTA in internal solution for *mdx* FDB fibres, and $54 \pm 13\%$ for *mdx* EDL fibres in the presence of 5 mM EGTA in the cut ends, compared to the respective normal counterparts.

AP-evoked fluorescence transients recorded with a high affinity Ca^{2+} indicator from FDB fibres

In contrast to the significant decrease in the amplitude of AP-evoked Ca^{2+} signals in *mdx* compared to normal fibres described above, previous studies have reported that Ca^{2+} transients were similar in the two strains of mice (Turner *et al.* 1991; Head, 1993; Tutdibi *et al.* 1999). However, all these studies used high affinity Ca^{2+} indicators (Fura-2 and Indo-1) in the absence of EGTA to measure Ca^{2+} transients. In an attempt to emulate these conditions, we examined the properties of AP-evoked Ca^{2+} signals in FDB fibres loaded with 50 μM OGB-1, a closely related analogue of OGB-5N with a significantly higher affinity for Ca^{2+} (see Methods), and no EGTA. It was necessary to include 50 μM BTS in the external solution to block contraction, as discussed above (Fig. 3). Panels *A* and *B* in Figure 5 show an AP superimposed on the evoked OGB-1 fluorescence transient from a normal and an *mdx* FDB fibre, respectively, recorded under these conditions. In agreement with our OGB-5N results in 0 EGTA (Fig. 4), the $(\Delta F/F)_{peak}$ of the OGB-1 transient was smaller in an *mdx* fibre (Fig. 5*B*) than in a normal fibre (Fig. 5*A*). As expected, though, because of the slowness of the indicator, the time course of both transients was longer (see Fig. 5 legend for values) than the corresponding OGB-5N transients (Fig. 4*A* and *B*). In addition, it can be observed that in the case of the normal fibre, the transient decays with an early sloping plateau phase followed by a late decay,

findings which are consistent with the possibility that OGB-1 is near saturation at the peak of the transient. These misrepresentations of the time course of the underlying Ca^{2+} signals makes a comparison between normal and *mdx* OGB-1 transients less valuable. For example, the clear prolongation in the FDHM of OGB-5N transients from *mdx* fibres without EGTA in the internal solution (Table 2, column 2) is no longer significantly manifested in OGB-1 transients recorded under similar conditions (50 ± 6 ms *versus* 68 ± 11 ms, $n = 5$ fibres from 2 normal mice *versus* $n = 6$ fibres from 2 *mdx* mice, respectively). Nevertheless, in agreement with all of the other data in this report, we found that OGB-1 transients from *mdx* fibres displayed a highly significant $36 \pm 6\%$ ($P < 0.0001$) decrease in the $(\Delta F/F)_{peak}$ compared to that of normal transients (*n* values as above for normal and *mdx* experiments).

Discussion

The pathophysiology of DMD is poorly understood. In particular, the weakness observed in isolated fibres from *mdx* mice and DMD patients has not been fully explained (Emery, 1993; Watchko *et al.* 2002). These results could be explained by lower evoked myoplasmic free $[Ca^{2+}]$ changes in dystrophic fibres. In contrast to previous reports (Turner *et al.* 1991; Head, 1993; Tutdibi *et al.* 1999), we demonstrate that *mdx* skeletal muscle fibres display a significant impairment in AP-evoked SR Ca^{2+} signalling which may provide a mechanism for the observed contractile dysfunction of these mice, and potentially for impaired force production of humans afflicted with DMD.

We began these studies using FDB muscles fibres obtained by collagenase dissociation since this afforded us high yields of twitching normal and *mdx* fibres. Since these FDB fibres are too short for gap isolation procedures, we developed a microelectrode-based technique for electrical and fluorescence recording. Similar to an approach used previously (Eusebi *et al.* 1980), we used two microelectrodes, one for loading the fibre with internal solution and passing current and the second for recording V_m without distortion.

In order to achieve accurate measurements of both optical and electrical signals, it was critical that fibre movement was arrested. To accomplish this, we used two different approaches. On the one hand, we included millimolar concentrations of EGTA in the internal solution for FDB fibres (or in the cut ends for EDL fibres). It has been reported previously that high intracellular [EGTA] reduces the amplitude, accelerates the time course, and constrains the free myoplasmic $[Ca^{2+}]$ changes to narrow regions circumscribing the Ca^{2+} release sites (Pape *et al.* 1995; DiGregorio *et al.* 1999; Novo *et al.* 2003). Empirically, the results reported here confirm these facts since fibres electrically stimulated in the absence of EGTA contracted vigorously, while those in the presence of ≥ 5 mM EGTA did not contract. Thus, the relatively large calculated $[Ca^{2+}]$ changes in the presence of EGTA (up to 4 μM peak $[Ca^{2+}]$) reported above did not occur throughout the myofibril and/or were brief enough to prevent the effective activation

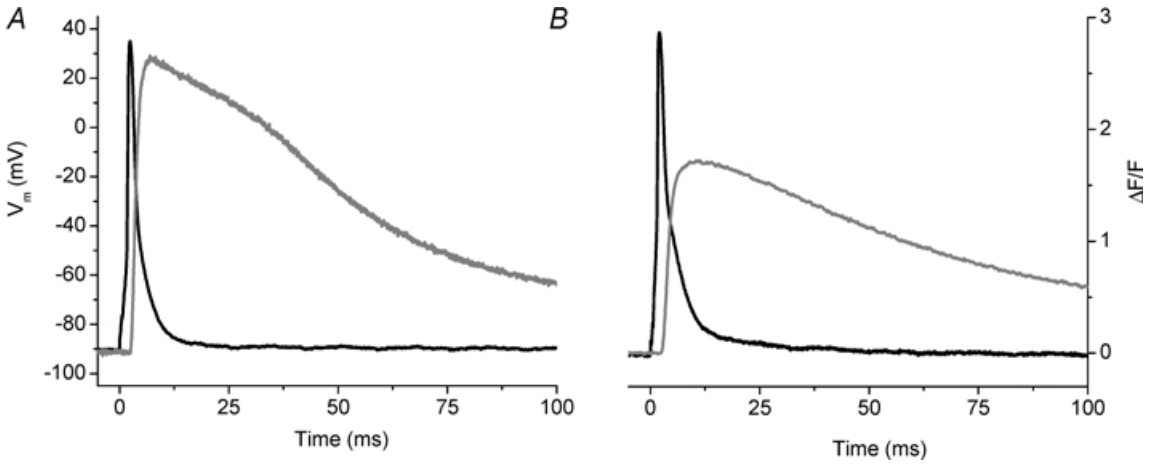

Figure 5. AP and evoked OGB-1 global transients from normal and *mdx* FDB fibres
A, superimposed AP (black) and evoked OGB-1 fluorescence transient (grey) from a 16-week-old normal FDB fibre loaded with 0.05 mM OGB-1 and in the presence of 50 μM extracellular BTS. $(\Delta F/F)_{peak} = 2.7$, $t_p = 4.32$ ms, FDHM = 50 ms. Fibre diameter = 31 μm. *B*, superimposed AP (black) and evoked OGB-5N fluorescence transient (grey) from a 12-week-old *mdx* FDB fibre loaded with 0.05 mM OGB-1 and in the presence of 50 μM extracellular BTS. $(\Delta F/F)_{peak} = 1.7$, $t_p = 8.0$ ms, FDHM = 65 ms. Fibre diameter = 29 μm. For all panels, $t = 0$ corresponds to the onset of stimulation.

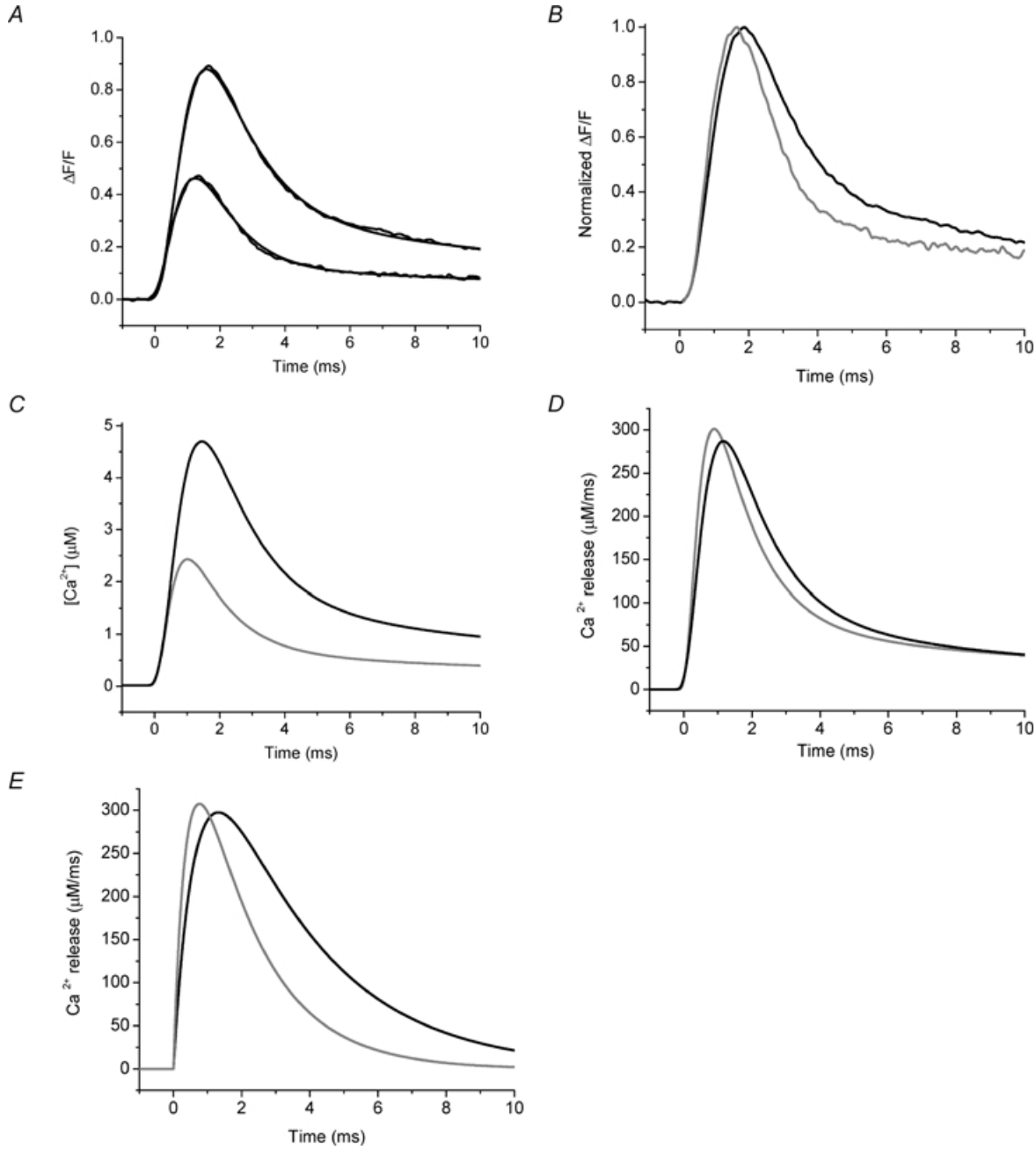

Figure 6. AP-evoked and simulated OGB-5N global transients from normal FDB fibre at different EGTA concentrations

A, AP-evoked OGB-5N transients recorded in the presence of 5 and 10 mM EGTA (larger and smaller black traces, respectively). The data were fitted to the predictions (grey traces) from a single compartment model in which the concentrations of OGB-5N and [EGTA] were those use in the experiments. The Ca^{2+} release function is described in the Methods. The fitted parameters (J_{max}, N, τ_1, τ_2, τ_3, τ_4, A_1, A_2, A_3) were, respectively, 103 μM ms^{-1}, 4.6, 0.5 ms, 1.3 ms, 1.2 ms, 13.4 ms, 3.8, 5, 0.9 for the 5 mM transient and 149 μM ms^{-1}, 5, 0.3 ms, 4 ms, 1.5 ms, 22 ms, 0.1, 3.8, 0.4 for the 10 mM transient. *B,* same $\Delta F/F$ transients as shown in Fig. 6*A* without fits shown normalized to their respective $(\Delta F/F)_{peaks}$. *C*, model predictions for the $[Ca^{2+}]$ changes in 5 mM (larger black trace) and 10 mM (smaller grey trace) EGTA as calculated from the single compartment model. *D*, Ca^{2+} release fluxes associated with the $[Ca^{2+}]$ change in 5 mM (black) and 10 mM (grey) EGTA presented in *C*, as calculated from the single compartment model. *E*, Ca^{2+} release fluxes associated with the $[Ca^{2+}]$ change in 5 mM (black) and 10 mM (grey) EGTA presented in *C*, as calculated from eqn (5) of Song *et al.* (1998). For *A*, APs were recorded but are not shown. For all panels, $t = 0$ corresponds to the start of each transient.

of the Ca^{2+} dependent conformational change by troponin in the region of actin/myosin overlap. Indeed, since the measured fluorescence change arises from small regions of the myofibril, whereas the baseline fluorescence arises from the entire myofibril, it is likely that the true local value of the peak $[Ca^{2+}]$ is significantly larger than the values reported in Table 1. Second, for experiments done in the absence of EGTA, we pharmacologically blocked contraction by adding BTS, a specific inhibitor of the muscle myosin ATPase (Cheung *et al.* 2002), to the extracellular solution. We extended the study by Cheung and collaborators by demonstrating that BTS is also an effective blocker of AP-evoked contraction in mammalian muscle fibres at a concentration of 50 μM without having any obvious impact on Ca^{2+} signalling of these fibres. It is worth noting, however, that an ~3-fold increase in the current necessary to maintain the resting V_m, and a prolongation of the falling phase of the AP was observed under these conditions.

A key finding of this report is that the amplitude of the AP-evoked OGB-5N transients of *mdx* muscle fibres was significantly decreased by ~40% compared to normal fibres with no difference in the AP. This decrease was observed in the presence and absence of intracellular EGTA, and therefore presumably at different resting free myoplasmic $[Ca^{2+}]$, as well as with high and low affinity indicators. Moreover, this decrement in the Ca^{2+} signalling of FDB fibres from *mdx* mice was also observed in EDL fibres loaded with 5 mM EGTA. Another major finding was that in the absence of EGTA, the decay phase of Ca^{2+} transients from *mdx* FDB fibres was significantly prolonged compared to normal fibres, in agreement with a previous report using a high affinity indicator (Turner *et al.* 1988). It should be emphasized that since there was no difference between our measurements of the surface AP in normal and *mdx* fibres, these alterations in AP-evoked Ca^{2+} signalling were measured in electrically indistinguishable populations of fibres. Moreover, all of our experiments were done in animals between 8 and 18 weeks of age, which corresponds to the postnecrotic phase of the *mdx* phenotype (McArdle *et al.* 1995). We found that within this age range there is little dispersion in the properties of the AP-evoked Ca^{2+} transients, as evidenced by the small value of the S.E.M. within each strain of mouse (Tables 1 and 2). Thus, we believe that the measured alterations in *mdx* Ca^{2+} signalling represent a physiologically relevant impairment in the excitation–contraction (EC) coupling process of dystrophic mice.

As mentioned above, this report contradicts a number of previous reports on *mdx* muscle AP Ca^{2+} signalling (Turner *et al.* 1988; Head, 1993; Tutdibi *et al.* 1999). In our view, these studies have a number of limitations which may affect the findings. First, these studies used high affinity indicators which may not have been able to track accurately in skeletal muscle fibres rapid $[Ca^{2+}]$ changes (Hirota *et al.* 1989; Escobar *et al.* 1997). To test whether a similar high affinity indicator missed the depression in the $(\Delta F/F)_{peak}$ of *mdx* fibres observed using OGB-5N, we repeated our measurements using the high affinity indicator OGB-1 in the absence of EGTA (Fig. 5*A* and *B*). The $\Delta F/F$ transients obtained from normal fibres using OGB-1 (Fig. 5*A*) suggest that the myoplasmic free $[Ca^{2+}]$ changes in response to AP stimulation in these fibres are large enough to approach the region of saturation for OGB-1. However, we still observed a similar reduction in the $(\Delta F/F)_{peak}$ of the *mdx* fibre transients under these conditions. Second, two of the previous studies presented calibrated Ca^{2+} transients obtained with Fura-2 and Indo-1 using an equation (Grynkiewicz *et al.* 1985) which assumes that the dye is at equilibrium with the free $[Ca^{2+}]$ (Turner *et al.* 1988; Head, 1993). This assumption is known to be in error for high affinity indicators (Escobar *et al.* 1997). Because of this error, we chose not to deconvolve the OGB-1 transients using similar assumptions, but we did so for the low affinity indicator OGB-5N since it has been demonstrated to be at near equilibrium with AP-evoked free $[Ca^{2+}]$ changes (Escobar *et al.* 1997). Thus, it is not possible for us to compare directly our high affinity transients with theirs. Nevertheless, we calculated peak $[Ca^{2+}]$ for normal and *mdx* fibres of 6.0 and 3.3 μM, respectively, in 0 EGTA (Table 2, columns 2 and 3). These values are up to 10-fold higher than those previously published for comparisons between *mdx* and normal fibres (Turner *et al.* 1991; Head, 1993; Tutdibi *et al.* 1999). In fact, our prediction for the peak $[Ca^{2+}]$ in *mdx* fibres in response to AP stimulation is considerably higher than those reported for normal fibres in these previous studies. In addition, our values are more in line with values reported for mammalian muscle fibres using low affinity indicators (Delbono & Stefani, 1993; Hollingworth *et al.* 1996). Another weakness of these studies is that they did not provide simultaneous measurements of the AP and the evoked Ca^{2+} signals (Turner *et al.* 1988; Head, 1993; Tutdibi *et al.* 1999). We measured both of these signals simultaneously and found that the surface AP is not altered in *mdx* fibres. This observation extends previous findings that both the passive electrical properties (Hollingworth *et al.* 1990) and the major conductances responsible for the AP are similar in the two strains of mice (Mathes *et al.* 1991; Hocherman & Bezanilla, 1996).

Because the impairments in Ca^{2+} signalling of *mdx* fibres we have reported here could result from an alteration

in the evoked SR Ca^{2+} release time course and/or the Ca^{2+} buffering/sequestration properties of these fibres, it is important to clarify the potential contributions of these two processes. It is worth emphasizing that, along with blocking contraction, another advantage of using high EGTA to study AP-evoked Ca^{2+} transients is that the endogenous buffering capacity of the fibres can be dominated. In turn, under this condition, the measured Ca^{2+} transient is representative of the AP-evoked SR Ca^{2+} release flux and, thus, any differences between the transients of normal and *mdx* mice represent differences in the properties of the release flux alone. The validity of this approach has been demonstrated in cardiac and skeletal muscle by using high intracellular [EGTA] and OGB-5N (Song *et al.* 1998; DiFranco *et al.* 2002; Novo *et al.* 2003). As discussed in the Methods section, it is unlikely that the [EGTA] in the impaled fibre in these studies was able to reach the pipette [EGTA]. However, the dramatic reduction of the FDHM for OGB-5N transients measured in the presence of 5 mM EGTA in the internal solution (Table 1), compared with the values in the absence of EGTA (Table 2), along with the concomitant blockage of contraction, suggests that a situation is reached where the exogenous buffer overwhelms the endogenous buffering capacity of the fibre. To assess this more directly, we compared the rates of release predicted by our kinetic model for the two internal solution EGTA concentrations. Figure 6*A* shows superimposed representative AP-evoked OGB-5N transients recorded from normal FDB fibres in the presence of 5 mM (larger black trace) and 10 mM (smaller black trace) EGTA. The $(\Delta F/F)_{peak}$ in 10 mM EGTA was decreased by 53% compared with that in 5 mM EGTA. Figure 6*B* shows the $\Delta F/F$ transients presented in Fig. 6*A* normalized to their respective maxima. Since the time courses of these two transients are similar, but much faster than those observed in the absence of EGTA (see Fig. 4*A* and Table 2), it is possible to suggest that 5 mM EGTA in the internal solution may be sufficient to unmask the time course of the flux itself. In order to more quantitatively analyse this possibility, $\Delta F/F$ transients were simulated by our kinetic model (see Methods) using adjustable Ca^{2+} release waveforms. Results designed to simulate the measured $\Delta F/F$ traces are superimposed on these experimental data (Fig. 6*A*). The predicted free $[Ca^{2+}]$ changes are shown in Fig. 6*C*. As expected, the model predicted smaller free $[Ca^{2+}]$ changes for the higher [EGTA] used but, importantly, the predicted fluxes for the 5 and 10 mM conditions were very similar (Fig. 6*D*). Moreover, when this analysis was performed using the analytical approximation of Song and collaborators (eqn (5) in Song *et al.* 1998), the predicted Ca^{2+} release fluxes were also very similar to each other and to our model predictions (compare Figs 6*D* and *E*). While the absolute values of the fluxes may be incorrect because of the uncertainty about the exact myoplasmic [EGTA], it is clear that the kinetics of the OGB-5N $\Delta F/F$ transients measured with 5 mM [EGTA] in the internal solution approximate the underlying AP-evoked SR Ca^{2+} release flux. Therefore, the decrease in the amplitude of the AP-evoked Ca^{2+} transients observed in *mdx* mice in the presence of high [EGTA] (Figs 2*B* and 3*B*) reflects an intrinsic impairment in the AP-evoked SR Ca^{2+} release flux of these mice. By deconvolving these $\Delta F/F$ transients using our kinetic model, we calculate that the AP-evoked SR Ca^{2+} release flux goes from 230 ± 22 μM ms^{-1} in normal fibres to 125 ± 12 μM ms^{-1} in *mdx* fibres ($n = 12$ fibres from 7 normal mice, $n = 17$ fibres from 7 *mdx* mice), which represents a 46 ± 9% flux reduction in dystrophic fibres. We can infer that, most likely, this decrement in the flux is also the cause of the decreased signals observed in 0 EGTA (Figs 4 and 5), but model simulations for this case will depend on the dynamic endogenous buffering in these fibres which, at present, has not been quantitatively characterized (see below).

Since we measured spatially averaged, multisarcomeric, Ca^{2+} signals, we cannot distinguish between the possibilities that all of the Ca^{2+} 'release units' are impaired to the same degree, or that there is a mixture of functioning and non-functioning units in different sarcomeres of *mdx* fibres. To evaluate these possibilities, a detailed exploration of the spatio-temporal evolution of the $[Ca^{2+}]$ changes with intrasarcomeric resolution, akin to what we have accomplished previously in amphibian fibres (DiFranco *et al.* 2002; Novo *et al.* 2003), will be required for normal and *mdx* fibres. It will also be important to identify where in the cascade of events responsible for EC coupling the impairment occurs. It seems unlikely that the voltage sensitivity of the release process is different in *mdx* mice since we observed no difference in the kinetics of the Ca^{2+} transients in 5 mM EGTA (which approximate the kinetics of the release process) (Figs 2 and 3, Table 1) and since charge movements have been reported to be normal in dystrophic fibres (Hollingworth *et al.* 1990). Thus, it is intriguing to suggest that the cause of the reduced AP-evoked Ca^{2+} release reported here for *mdx* fibres occurs after the voltage-dependent coupling at the triads and there is both biochemical and physiological evidence in support of this possible explanation (Hoffman *et al.* 1987*b*; Knudson *et al.* 1988; Culligan *et al.* 2002; Friedrich *et al.* 2003). Alternatively, an explanation for

this impairment may be that the T-tubule system is altered in *mdx* mice and we are currently investigating this issue.

The longer decay phase of *mdx* fibres observed with both indicators in the absence of intracellular EGTA (Fig. 4) suggests that *mdx* and normal fibres have different mechanisms of myoplasmic Ca^{2+} binding and/or subsequent sequestration by the SR. A possible explanation for the prolongation of the decay phase is the reduction in the parvalbumin protein content of *mdx* fibres, as reported previously (Sano *et al.* 1990), a decrease which has been reported for other adult dystrophic muscles as well (Klug *et al.* 1985). In addition, or alternatively, our results could be explained by the apparent reduction in the maximal velocity of Ca^{2+} transport by the SR Ca^{2+} pump in *mdx* mice (Kargacin & Kargacin, 1996). Fibres from *mdx* mice have been reported to have a higher proportion of slow (type I) fibres (Petrof *et al.* 1993) and it could be argued that the prolongation of the decay phase of *mdx* transients reported here is representative of this. We feel that this is unlikely, however, since the prolongation in the decay phase of the *mdx* fibre transients compared to normal fibre transients, recorded using OGB-5N in the absence of EGTA, is much greater than that shown in a previous study for slow fibres compared to fast fibres (Baylor & Hollingworth, 2003). Moreover, since BTS was effective at relatively low concentrations, it is likely that the *mdx* fibres used here were fast-twitch fibres, since slow-twitch fibres express the β-forms of myosin II, which is much less sensitive to BTS (Cheung *et al.* 2002). It is clear, however, that this alteration of Ca^{2+} signalling in *mdx* fibres is hidden when experiments are performed with 5 mM EGTA in internal solution since the kinetics of the transients from normal and *mdx* fibres are statistically similar under this condition (Table 1 and Figs 2 and 3). Whatever the cause, the prolongation of the decay phase of the AP-evoked Ca^{2+} transient of *mdx* fibres may explain the lengthening of the relaxation time of dystrophic muscle contraction (Parslow & Parry, 1981; Bressler *et al.* 1983; Dangain & Vrbova, 1984).

Finally, it will be important to examine AP-evoked SR Ca^{2+} release in fibres of young *mdx* mice ($<$ 4 weeks of age) which are in the prenecrotic phase of development (Head *et al.* 1992; Gillis, 1999; Durbeej & Campbell, 2002) in order to clarify whether the pathophysiology caused by the absence of dystrophin leads to the impaired AP-evoked Ca^{2+} signalling we have observed either directly or indirectly by affecting the subsequent development muscle fibres in *mdx* mice.

References

Baylor SM & Hollingworth S (2003). Sarcoplasmic reticulum calcium release compared in slow-twitch and fast-twitch fibres of mouse muscle. *J Physiol* **551**, 125–138.

Bers DM, Patton CW & Nuccitelli R (1994). A practical guide to the preparation of Ca2+ buffers. *Meth Cell Biol* **40**, 3–29.

Bressler BH, Jasch LG, Ovalle WK & Slonecker CE (1983). Changes in isometric contractile properties of fast-twitch and slow-twitch skeletal muscle of C57BL/6J dy2J/dy2J dystrophic mice during postnatal development. *Exp Neurol* **80**, 457–470.

Cheung A, Dantzig JA, Hollingworth S, Baylor SM, Goldman YE, Mitchison TJ & Straight AF (2002). A small-molecule inhibitor of skeletal muscle myosin II. *Nat Cell Biol* **4**, 83–88.

Coirault C, Lambert F, Marchand-Adam S, Attal P, Chemla D & Lecarpentier Y (1999). Myosin molecular motor dysfunction in dystrophic mouse diaphragm. *Am J Physiol* **277**, C1170–C1176.

Culligan K, Banville N, Dowling P & Ohlendieck K (2002). Drastic reduction of calsequestrin-like proteins and impaired calcium binding in dystrophic mdx muscle. *J Appl Physiol* **92**, 435–445.

Dangain J & Vrbova G (1984). Muscle development in mdx mutant mice. *Muscle Nerve* **7**, 700–704.

Delbono O & Stefani E (1993). Calcium transients in single mammalian skeletal muscle fibres. *J Physiol* **463**, 689–707.

DiFranco M, Novo D & Vergara J (2002). Characterization of the calcium release domains during excitation contraction coupling in skeletal muscle fibres. *Pflugers Arch* **443**, 508–519.

DiGregorio DA, Peskoff A & Vergara JL (1999). Measurement of action potential-induced presynaptic calcium domains at a cultured neuromuscular junction. *J Neurosci* **19**, 7846–7859.

Durbeej M & Campbell KP (2002). Muscular dystrophies involving the dystrophin-glycoprotein complex: an overview of current mouse models. *Curr Opin Genet Dev* **12**, 349–361.

Emery AEH (1993). *Duchenne Muscular Dystrophy*. Oxford University Press, Oxford; New York.

Emery AE (2002). The muscular dystrophies. *Lancet* **359**, 687–695.

Escobar AL, Cifuentes F & Vergara JL (1995). Detection of Ca(2+)-transients elicited by flash photolysis of DM-nitrophen with a fast calcium indicator. *FEBS Lett* **364**, 335–338.

Escobar AL, Velez P, Kim AM, Cifuentes F, Fill M & Vergara JL (1997). Kinetic properties of DM-nitrophen and calcium indicators: rapid transient response to flash photolysis. *Pflugers Arch* **434**, 615–631.

Eusebi F, Miledi R & Takahashi T (1980). Calcium transients in mammalian muscles. *Nature* **284**, 560–561.

Fink RH, Stephenson DG & Williams DA (1990). Physiological properties of skinned fibres from normal and dystrophic (Duchenne) human muscle activated by Ca^{2+} and Sr^{2+}. *J Physiol* **420**, 337–353.

Friedrich O, Both M, Gillis JM, Chamberlain JS & Fink RH (2003). Mini-dystrophin restores L-type calcium currents in skeletal muscle of transgenic mdx mice. *J Physiol* **555**, 251–265.

Gillis JM (1999). Understanding dystrophinopathies: an inventory of the structural and functional consequences of the absence of dystrophin in muscles of the mdx mouse. *J Muscle Res Cell Motil* **20**, 605–625.

Godt RE (1974). Calcium-activated tension of skinned muscle fibers of the frog. Dependence on magnesium adenosine triphosphate concentration. *J General Physiol* **63**, 722–739.

Grynkiewicz G, Poenie M & Tsien RY (1985). A new generation of Ca2+ indicators with greatly improved fluorescence properties. *J Biol Chem* **260**, 3440–3450.

Head SI (1993). Membrane potential, resting calcium and calcium transients in isolated muscle fibres from normal and dystrophic mice. *J Physiol* **469**, 11–19.

Head SI, Stephenson DG & Williams DA (1990). Properties of enzymatically isolated skeletal fibres from mice with muscular dystrophy. *J Physiol* **422**, 351–367.

Head SI, Williams DA & Stephenson DG (1992). Abnormalities in structure and function of limb skeletal muscle fibres of dystrophic mdx mice. *Proc R Soc Lond B Biol Sci* **248**, 163–169.

Hille B & Campbell DT (1976). An improved vaseline gap voltage clamp for skeletal muscle fibers. *J General Physiol* **67**, 265–293.

Hirota A, Chandler WK, Southwick PL & Waggoner AS (1989). Calcium signals recorded from two new purpurate indicators inside frog cut twitch fibers. *J General Physiol* **94**, 597–631.

Hocherman SD & Bezanilla F (1996). A patch-clamp study of delayed rectifier currents in skeletal muscle of control and *mdx* mice. *J Physiol* **493**, 113–128.

Hoffman EP, Brown RH Jr & Kunkel LM (1987*a*). Dystrophin: the protein product of the Duchenne muscular dystrophy locus. *Cell* **51**, 919–928.

Hoffman EP, Knudson CM, Campbell KP & Kunkel LM (1987*b*). Subcellular fractionation of dystrophin to the triads of skeletal muscle. *Nature* **330**, 754–758.

Hollingworth S, Marshall MW & Robson E (1990). Excitation contraction coupling in normal and mdx mice. *Muscle Nerve* **13**, 16–20.

Hollingworth S, Zhao M & Baylor SM (1996). The amplitude and time course of the myoplasmic free [Ca2+] transient in fast-twitch fibers of mouse muscle. *J General Physiol* **108**, 455–469.

Kargacin ME & Kargacin GJ (1996). The sarcoplasmic reticulum calcium pump is functionally altered in dystrophic muscle. *Biochim Biophys Acta* **1290**, 4–8.

Kim AM & Vergara JL (1998). Fast voltage gating of Ca^{2+} release in frog skeletal muscle revealed by supercharging pulses. *J Physiol* **511**, 509–518.

Klug G, Reichmann H & Pette D (1985). Decreased parvalbumin contents in skeletal muscles of C57BL/6J (dy2J/dy2J) dystrophic mice. *Muscle Nerve* **8**, 576–579.

Knudson CM, Hoffman EP, Kahl SD, Kunkel LM & Campbell KP (1988). Evidence for the association of dystrophin with the transverse tubular system in skeletal muscle. *J Biol Chem* **263**, 8480–8484.

McArdle A, Edwards RH & Jackson MJ (1995). How does dystrophin deficiency lead to muscle degeneration? – evidence from the mdx mouse. *Neuromuscul Disord* **5**, 445–456.

Mathes C, Bezanilla F & Weiss RE (1991). Sodium current and membrane potential in EDL muscle fibers from normal and dystrophic (mdx) mice. *Am J Physiol* **261**, C718–C725.

Mathias RT, Cohen IS & Oliva C (1990). Limitations of the whole cell patch clamp technique in the control of intracellular concentrations. *Biophys J* **58**, 759–770.

Maylie J, Irving M, Sizto NL & Chandler WK (1987). Comparison of arsenazo III optical signals in intact and cut frog twitch fibers. *J General Physiol* **89**, 41–81.

Melzer W, Rios E & Schneider MF (1987). A general procedure for determining the rate of calcium release from the sarcoplasmic reticulum in skeletal muscle fibers. *Biophys J* **51**, 849–863.

Nagerl UV, Novo D, Mody I & Vergara JL (2000). Binding kinetics of calbindin-D (28k) determined by flash photolysis of caged Ca(2+). *Biophys J* **79**, 3009–3018.

Novo D, DiFranco M & Vergara JL (2003). Comparison between the predictions of diffusion-reaction models and localized Ca2+ transients in amphibian skeletal muscle fibers. *Biophys J* **85**, 1080–1097.

Palade P & Vergara J (1982). Arsenazo III and antipyrylazo III calcium transients in single skeletal muscle fibers. *J General Physiol* **79**, 679–707.

Pape PC, Jong DS & Chandler WK (1995). Calcium release and its voltage dependence in frog cut muscle fibers equilibrated with 20 mM EGTA. *J General Physiol* **106**, 259–336.

Parry DJ & Parslow HG (1981). Fiber type susceptibility in the dystrophic mouse. *Exp Neurol* **73**, 674–685.

Parslow HG & Parry DJ (1981). Slowing of fast-twitch muscle in the dystrophic mouse. *Exp Neurol* **73**, 686–699.

Petrof BJ, Stedman HH, Shrager JB, Eby J, Sweeney HL & Kelly AM (1993). Adaptations in myosin heavy chain expression and contractile function in dystrophic mouse diaphragm. *Am J Physiol* **265**, C834–C841.

Pusch M & Neher E (1988). Rates of diffusional exchange between small cells and a measuring patch pipette. *Pflugers Arch* **411**, 204–211.

Raymackers JM, Gailly P, Schoor MC, Pette D, Schwaller B, Hunziker W, Celio MR & Gillis JM (2000). Tetanus relaxation of fast skeletal muscles of the mouse made parvalbumin deficient by gene inactivation. *J Physiol* **527**, 355–364.

Sano M, Yokota T, Endo T & Tsukagoshi H (1990). A developmental change in the content of parvalbumin in normal and dystrophic mouse (mdx) muscle. *J Neurol Sci* **97**, 261–272.

Shaw MA, Ostap EM & Goldman YE (2003). Mechanism of inhibition of skeletal muscle actomyosin by N-benzyl-p-toluenesulfonamide. *Biochemistry* **42**, 6128–6135.

Song L-S, Sham JSK, Stern MD, Lakatta EG & Cheng H (1998). Direct measurement of SR release flux by tracking 'Ca spikes' in rat cardiac myocytes. *J Physiol* **512**, 677–691.

Szentesi P, Jacquemond V, Kovacs L & Csernoch L (1997). Intramembrane charge movement and sarcoplasmic calcium release in enzymatically isolated mammalian skeletal muscle fibres. *J Physiol* **505**, 371–384.

Turner PR, Fong PY, Denetclaw WF & Steinhardt RA (1991). Increased calcium influx in dystrophic muscle. *J Cell Biol* **115**, 1701–1712.

Turner PR, Westwood T, Regen CM & Steinhardt RA (1988). Increased protein degradation results from elevated free calcium levels found in muscle from mdx mice. *Nature* **335**, 735–738.

Tutdibi O, Brinkmeier H, Rudel R & Fohr KJ (1999). Increased calcium entry into dystrophin-deficient muscle fibres of MDX and ADR-MDX mice is reduced by ion channel blockers. *J Physiol* **515**, 859–868.

Vergara J & DiFranco M (1992). Imaging of calcium transients during excitation-contraction coupling in skeletal muscle fibers. *Adv Exp Med Biol* **311**, 227–236.

Vergara JL, DiFranco M & Novo D (2001). Dimensions of calcium release domains in frog skeletal muscle fibers. *Proc SPIE* **4259**, 133–143.

Wang ZM, Messi ML & Delbono O (1999). Patch-clamp recording of charge movement, Ca(2+) current, and Ca(2+) transients in adult skeletal muscle fibers. *Biophys J* **77**, 2709–2716.

Watchko JF, O'Day TL & Hoffman EP (2002). Functional characteristics of dystrophic skeletal muscle: insights from animal models. *J Appl Physiol* **93**, 407–417.

Wood DS, Sorenson MM, Eastwood AB, Charash WE & Reuben JP (1978). Duchenne dystrophy: abnormal generation of tension and Ca++ regulation in single skinned fibers. *Neurology* **28**, 447–457.

Woods CE, Novo D & Vergara J (2003). Global calcium transients in normal and dystrophic muscle fibers. *Biophysical Society Meeting* **84**, 572a.

Woods CE & Vergara JL (2002). A combined method for confocal detection of Ca2+ signals and fluorescence-recovery-after-photobleaching (FRAP). *Biophys J (Annu Meeting Abstracts)* **82**, 278a.

Acknowledgements

The authors thank A. Grinnell and J. Tidball for their helpful comments and discussions on a previous version of the manuscript. We would also like to thank B. Criswell for help with muscle fibre preparation and G. Faas for help with *in vitro* $[Ca^{2+}]$ calibrations. C.E.W. was partially supported by National Institutes of Health Training Grant GM08042 (UCLA MSTP). This work was supported by National Institutes of Health grants AR25201 and AR47664, a Grant in Aid from the Muscular Dystrophy Association, and a UC MEXUS grant to J.L.V., and a National Science and Engineering Research Council fellowship PGSB-242387- 2001, Canada, to D.N.